NEURAL REGENERATION RESEARCH
www.nrronline.org

Research Article

# Effects of amyloid precursor protein peptide APP96-110, alone or with human mesenchymal stromal cells, on recovery after spinal cord injury

https://doi.org/10.4103/1673-5374.327357
Date of submission: October 28, 2020
Date of decision: December 14, 2020
Date of acceptance: January 4, 2021
Date of web publication: November 12, 2021

Stuart I. Hodgetts[1, 2, *], Sarah J. Lovett[1], D. Baron-Heeris[1], A. Fogliani[1], Marian Sturm[3], C. Van den Heuvel[4], Alan R. Harvey[1, 2]

## From the Contents



**Graphical Abstract** *Amyloid precursor protein peptide APP96-110 may provide neuroprotection to improve morphological and functional outcomes after spinal cord injury which may be enhanced when combined with hMSC transplantation*

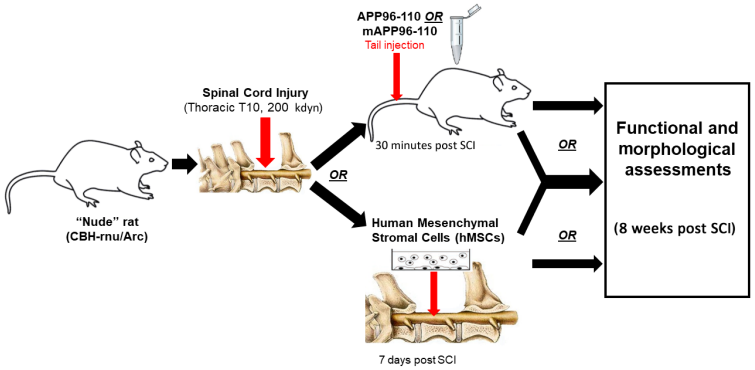


## Abstract

Delivery of a peptide (APP96-110), derived from amyloid precursor protein (APP), has been shown to elicit neuroprotective effects following cerebral stroke and traumatic brain injury. In this study, the effect of APP96-110 or a mutant version of this peptide (mAPP96-110) was assessed following moderate (200 kdyn, (2 N)) thoracic contusive spinal cord injury (SCI) in adult Nude rats. Animals received a single tail vein injection of APP96-110 or mAPP96-110 at 30 minutes post-SCI and were then assessed for functional improvements over the next 8 weeks. A cohort of animals also received transplants of either viable or non-viable human mesenchymal stromal cells (hMSCs) into the SC lesion site at one week post-injury to assess the effect of combining intravenous APP96-110 delivery with hMSC treatment. Rats were perfused 8 weeks post-SCI and longitudinal sections of spinal cord analyzed for a number of factors including hMSC viability, cyst size, axonal regrowth, glial reactivity and macrophage activation. Analysis of sensorimotor function revealed occasional significant differences between groups using Ladderwalk or Ratwalk tests, however there were no consistent improvements in functional outcome after any of the treatments. mAPP96-110 alone, and APP96-110 in combination with both viable and non-viable hMSCs significantly reduced cyst size compared to SCI alone. Combined treatments with donor hMSCs also significantly increased βIII tubulin$^+$, glial fibrillary acidic protein (GFAP$^+$) and laminin$^+$ expression, and decreased ED1$^+$ expression in tissues. This preliminary study demonstrates that intravenous delivery of APP96-110 peptide has selective, modest neuroprotective effects following SCI, which may be enhanced when combined with hMSC transplantation. However, the effects are less pronounced and less consistent compared to the protective morphological and cognitive impact that this same peptide has on neuronal survival and behaviour after stroke and traumatic brain injury. Thus while the efficacy of a particular therapeutic approach in one CNS injury model may provide justification for its use in other neurotrauma models, similar outcomes may not necessarily occur and more targeted approaches suited to location and severity are required. All animal experiments were approved by The University of Western Australia Animal Ethics Committee (RA3/100/1460) on April 12, 2016.

**Key Words:** amyloid precursor protein; cell transplantation; combination; contusion; functional recovery; mesenchymal stromal cells; neuroprotection; regeneration; spinal cord injury; tissue sparing

Chinese Library Classification No. R453; R364; R741

## Introduction

Secondary degenerative changes following an initial trauma are major contributors to the extensive cell death and tissue damage, and associated loss of functional connections, that occur after spinal cord injury (SCI) (Hausmann, 2003; Hagg and Oudega, 2006). Widespread and ongoing degenerative events create a hostile injury site that is unable to support cell survival, axonal regrowth/regeneration and remyelination

[1]School of Human Sciences, The University of Western Australia (UWA), Perth, WA, Australia; [2]Perron Institute for Neurological and Translational Science, Perth, WA, Australia; [3]Cell and Tissue Therapies WA (CTTWA), Royal Perth Hospital, Perth, WA, Australia; [4]Adelaide Medical School, Faculty of Health and Medical Sciences, The University of Adelaide, Adelaide, SA, Australia
***Correspondence to:** Stuart I. Hodgetts, PhD, stuart.hodgetts@uwa.edu.au.
https://orcid.org/0000-0002-3318-0410 (Stuart I. Hodgetts)

***Funding:*** *This work was supported by the Neurotrauma Research Program of Western Australia.*
***How to cite this article:*** *Hodgetts SI, Lovett SJ, Baron-Heeris D, Fogliani A, Sturm M, den Heuvel CV, Harvey AR (2022) Effects of amyloid precursor protein peptide APP96-110, alone or with human mesenchymal stromal cells, on recovery after spinal cord injury. Neural Regen Res 17(6):1376-1386.*

following injury. Any reduction in inflammatory damage and secondary degeneration may significantly improve neuronal and glial cell survival, thereby increasing tissue sparing and the preservation of functional connections at the lesion site, potentially resulting in functional and morphological improvements (Bethea and Dietrich, 2002; Alexander and Popovich, 2009; Bowes and Yip, 2014).

Many neuroprotective approaches aim to reduce host tissue damage following SCI by modulating inflammatory and immunological reactions at the lesion site, protecting neuronal and glial cells against excitotoxicity or by inhibiting apoptosis (Kwon et al., 2011; Siddiqui et al., 2015). Cationic arginine-rich peptides and polyarginine or arginine-rich peptides have potent neuroprotective properties *in vitro* (Meloni et al., 2014, 2015a, b; Edwards et al., 2017), and *in vivo* they have been shown to be protective after both permanent and transient middle cerebral artery occlusion (MCAO) stroke in rats (Meloni et al., 2015a, 2017; Milani et al., 2016, 2017). Derived from the apolipoprotein E and amyloid precursor proteins (APP) respectively, the COG1410 and APP96-110 peptides are cationic and arginine rich (Chiu et al., 2017) and also exhibit neuroprotective effects following traumatic brain injury (TBI) (Hoane et al., 2007; Laskowitz et al., 2007; Tukhovskaya et al., 2009; Kaufman et al., 2010; Jiang and Brody, 2012; Corrigan et al., 2014; Cao et al., 2016; Qin et al., 2017). The neuroprotective potential of APP has been studied in a number of central nervous system (CNS) injury models after it was identified that APP upregulation following traumatic brain injury (TBI) is associated with a significant increase in neuronal survival (Van den Heuvel et al., 1999). Further investigation of APP identified several functional regions that may contribute to its neuroprotective ability. In particular, the heparin binding site at amino acid residues 96-110 (APP96-110) was shown to have neuroprotective effects following TBI, resulting in reduced lesion volume and axonal injury, increased numbers of spared neurons, and improved functional and cognitive outcomes (Corrigan et al., 2011, 2014; Plummer et al., 2018). The APP96-110 peptide may also exert similar neuroprotective effects in other traumatic CNS injury models.

In the present study, the neuroprotective effect of APP96-110 was assessed following moderate contusive SCI in Nude rats (Hodgetts et al., 2013a, b), with animals given a single intravenous injection of APP96-110 (active) and mAPP96-110 (mutant; with reduced but not absent heparin binding ability (Corrigan et al., 2014)) peptides at 30 minutes post-SCI. Because multipotent mesenchymal stromal cells (MSCs) are anti-inflammatory and immunomodulatory (Gronthos et al., 2003; Herrmann et al., 2012; Herrmann and Sturm, 2014) and cells of this lineage have been shown to elicit beneficial effects after SCI (Tetzlaff et al., 2011; Hodgetts et al., 2013a, b), a cohort of animals also received transplantation of viable (v) or non-viable (nv) human mesenchymal stromal cells (hMSCs) at one week post-injury, to assess the effect of combined APP96-110 and hMSC treatment. Based on previous studies carried out in the brain (Van den Heuvel et al., 1999; Hoane et al., 2007; Laskowitz et al., 2007; Tukhovskaya et al., 2009; Kaufman et al., 2010; Jiang and Brody, 2012; Corrigan et al., 2014; Cao et al., 2016; Qin et al., 2017), it was hypothesised that APP96-110 will exert neuroprotective effects following SCI, leading to significantly reduced tissue damage, and improved tissue sparing and functional recovery. Combined treatment with hMSC transplantation will determine whether the altered local environment of the cell transplanted injury site provides an even better platform for the regrowth of axons after APP96-110-induced neuroprotection. This combined treatment may produce greater improvements than APP96-110 or hMSCs alone.

## Materials and Methods

### Experimental animals

All animal work was approved by The University of Western Australia Animal Ethics Committee (RA3/100/1460, approved on April 12, 2016) and conformed to National Health and Medical Research Council (Australia) guidelines. Fifty-one adult female CBH-rnu/Arc (Athymic Nude) rats (≥ 12 weeks, body weight 140–170 g; Animal Resources Centre, Perth, WA, Australia) were used in this study, distributed randomly across 8 experimental groups ($n$ = 4–8/group) as shown in **Table 1**. Animals were housed in filter top cages with absorbent bedding, with access to food and water *ad libitum*, on a 12-hour light-dark cycle (red lights on 1000–2200). Animals were acclimated to the holding room, handled and pre-trained on all behavioural testing apparatus daily for 2 weeks prior to SCI surgery.

**Table 1** | **Treatment groups and number of animals per group, sacrificed at 8 weeks post-injury**

| Treatment | *n* |
|---|---|
| SCI only | 6 |
| SCI + mAPP96-110 | 6 |
| SCI + APP96-110 | 6 |
| SCI + hMSCs | 6 |
| SCI + mAPP96-110 + hMSCs | 4 |
| SCI + APP96-110 + hMSCs | 8 |
| SCI + nv-hMSCs | 7 |
| SCI + APP96-110 + nv-hMSCs | 8 |

APP96-110: amyloid precursor protein; hMSCs: human mesenchymal stromal cells; mAPP96-100: mutant amyloid precursor protein; nv: non-viable; SCI: spinal cord injury.

### SCI

Pre-surgical buprenorphine (Temgesic, 1 µg/100 g body weight, 300 U/mL, intraperitoneal (i.p.); Reckitt Benckiser Healthcare, West Ryde, NSW, Australia) was administered 30 minutes prior to the induction of anaesthesia. Animals were anaesthetised with isoflurane (induced at 3–4% (v/v) and maintained at 1.5–2.5% (v/v); Bayer, Leverkusen, Germany) combined with nitrous oxide (60% (v/v); 4 L/min) and oxygen (38.5% (v/v); 2 L/min). Ophthalmic eye ointment was applied to the eyes to prevent drying during surgery. The back of the animal was shaved and the surgical site cleaned with 4% (w/v) chlorhexidine solution. Skin overlying the thoracic area and underlying musculature was cut, and excess muscle removed from the dorsal and lateral processes of the vertebrae. A partial laminectomy of the 10 vertebra was performed using Rongeurs (Fine Science Tools (FST), North Vancouver, BC, Canada) to expose the underlying spinal cord without disrupting the dura. Surrounding bone was cleared as needed to provide sufficient clearance for the impactor head to access the dorsal surface of the spinal cord. A moderate (200 kdyn (2 N)) contusive SCI was performed at the T10 level using an Infinite Horizon impactor (Precision Systems and Instrumentation; Lexington, KY, USA).

Following injury, muscles were sutured and the overlying skin was closed with wound clips (Michel Suture Clips; FST). Rehydrating normal saline (2 mL, subcutaneous (SC), 0.9% (w/v) sodium chloride; Baxter, Deerfield, IL, USA) and antibiotic Benacillin (0.02 mL/100 g body weight, 300 U/mL, intramuscular (i.m.; gastrocnemius), 150 mg/mL procaine penicillin, 150 mg/mL benzathine penicillin, 20 mg/mL procaine hydrochloride); Ilium, Troy Laboratories, Glendenning, NSW, Australia) were administered immediately following surgery. Animals were returned to clean cages and placed in a heating cabinet (26°C) for 24–48 hours post-surgery to aide recovery from anaesthesia. Normal saline (0.5–2 mL) and buprenorphine (0.25–1 µg/100 g body weight; dose

reduced every second day) were administered (SC) daily for 1 week post-surgery. To prevent bladder infection, antibiotic (Benacillin; 0.02 mL/100 g body weight) was administered (IM; alternating legs) every second day for 1 week post-surgery. Bladders were manually expressed twice daily for 2 weeks or until normal bladder function returned.

### Peptide treatment

Custom APP96-110 (active) and mAPP96-110 (mutant; with reduced heparin binding ability (Corrigan et al., 2014)) peptides were produced by Auspep Pty Ltd (Tullamarine, VIC, Australia) according to the sequences; APP96-110: AC-N W C K R G R K Q C K T H P H-NH2; mAPP96-110: AC-N W C N Q G G K Q C K T H P H-NH2). The APP96-110 peptide contained a disulphide bridge between cysteines 98 and 105, important for efficacy (Small et al., 1994; Corrigan et al., 2014). For animals that received peptide treatment (**Table 1**), a single intravenous injection of active or mutant peptide (0.05 mg/kg) in normal saline (Baxter) was administered via the tail vein at 30 minuntes post-SCI in accordance with previous literature (Plummer et al., 2018).

### hMSC culture

Clinical grade hMSCs were obtained from Cell and Tissue Therapies WA (CTTWA; Royal Perth Hospital, Perth, Western Australia, Australia) and had been isolated using methods similar to those described previously (Herrmann et al., 2012; Hodgetts et al., 2013a, b). Frozen hMSCs were rapidly thawed in a 37°C water bath, washed in minimum essential medium-alpha modification (α-MEM; Gibco, Thermo Fisher Scientific, Waltham, MA, USA) supplemented with 10% (v/v) foetal bovine serum (FBS; Gibco) and seeded into T75 flasks (Corning, St. Louis, MO, USA) at a concentration of 2.5–3.5 × $10^3$ cells/$cm^2$ in α-MEM/10% FBS. Cells were maintained in α-MEM/10% FBS and incubated at 37°C/5% (v/v) carbon dioxide ($CO_2$) for transplantation, or used for *in vitro* differentiation and characterisation studies.

### *In vitro* differentiation

To confirm multipotency *in vitro*, donor hMSCs were differentiated into osteoblasts, adipocytes and chondrocytes using StemXVivo Osteogenic/Adipogenic/Chondrogenic differentiation media (R&D Systems, Minneapolis, MN, USA) according to manufacturers' instructions. Differentiation was confirmed by staining fixed cells on microscope slides with 2% (w/v) Alizarin Red S (Sigma-Aldrich; osteoblasts), 0.3% (w/v) Oil Red O in isopropanol (Sigma-Aldrich; adipocytes), or 0.05% (w/v) Toluidine blue O (Sigma-Aldrich; chondrocytes) followed by solvent (e.g. acetone, xylene) dehydration.

### *In vitro* characterisation

Non-differentiated donor hMSCs were seeded onto 0.1 mg/mL (w/v) poly-L-lysine (PLL; Sigma-Aldrich)/0.05 mg/mL (w/v) laminin (Sigma-Aldrich) coated 8-well chamber slides, at a concentration of 1 × $10^4$ cells/well. Cells were grown to 80–90% confluence, fixed in 4% (w/v) paraformaldehyde (PFA; Sigma-Aldrich) and assessed for marker expression against the panel of antibodies outlined in **Table 2**.

### Preparation for cell transplantation

Donor hMSCs (passage 3–5) for spinal cord transplantation were used directly from culture. Once cells had grown to 80–90% confluence, flasks were washed 3× with Hanks' balanced salt solution (HBSS; Gibco), incubated with 0.05% Trypsin-EDTA (Gibco) for 3–5 minutes until adherent cells were detached from the flask surface, then cells were collected into fresh α-MEM/10% FBS. The cell suspension was centrifuged, supernatant discarded and the cell pellet resuspended in PBS (Gibco). Cell viability was determined using trypan blue (Sigma-Aldrich) staining, and the cell suspension was adjusted to a concentration of 6.25 × $10^4$ viable cells/μL. For non-viable (nv; control) cells (nv-hMSCs), prepared cell suspensions were repeatedly freeze-thawed in liquid nitrogen until the cells were no longer viable as indicated by trypan blue staining (< 5% viability after 4 freeze/thaw cycles). Non-viable hMSCs are an appropriate control to assess whether the effects of cell transplantation on experimental outcomes are due to the ongoing influence of any live engrafted donor cells remaining in the lesion site, in contrast to the simple addition of (inactive) cellular material that could modulate the transplantation site to provide a more favourable terrain for repair, regrowth and/or regeneration (Katoh et al., 2019). All cell suspensions were stored on ice prior to and for the duration of the transplantation surgery (viable cells remain ~90% viable after 6 hours on ice as determined by trypan blue staining).

**Table 2** | **Primary and secondary antibodies used for immunohistochemistry**

| Antibody | Host | Dilution | Manufacturer | Catalogue # | Lot # |
|---|---|---|---|---|---|
| **Primary antibody** | | | | | |
| Anti-Rat CD68 (ED1) | Ms | 1:250 | Bio-Rad | MCA341R | 1014 |
| Anti-GAP43 | Ms | 1:200 | Life Technologies | 33-5000 | QC214626 |
| Anti-GFAP | Rb | 1:1000 | Dako | Z0334 | 20025480 |
| Anti-Iba1 | Rb | 1:500 | Wako | 019-19741 | LKN4881 |
| Anti-Laminin (extracellular matrix) | Rb | 1:1000 | Sigma | L9393 | 015M4881V |
| Anti-Neurofilament H | Ms | 1:1000 | BioLegend | 801701 | B198916 |
| Anti-S100-β | Ms | 1:500 | Sigma | S2532 | 070M4767 |
| STEM101 | Ms | 1:200 | Cellartis | Y40400 | AF2L001 AF9L001 |
| Anti-βIII tubulin | Rb | 1:1500 | BioLegend | 802001 | B209045 |
| **Secondary antibody** | | | | | |
| Cy3 Anti-Ms | Gt | 1:500 | Jackson ImmunoResearch | 115-166-062 | 121709 |
| FITC Anti-Rb | Gt | 1:300 | Jackson ImmunoResearch | 111-096-045 | 122343 |

FITC: Fluorescein isothiocyanate; GAP43: growth associated protein-43; GFAP: glial fibrillary acidic protein; Gt: goat; Ms: mouse; nv: non-viable; Rb: rabbit.

### Cell transplantation

At 1 week post-injury, cohorts of animals received transplantation of either viable or non-viable (nv) hMSCs into the spinal cord lesion site (**Table 1**; 5 × $10^5$ cells in 8 μL PBS total). Animals were prepared for cell transplantation surgery and anaesthetised as described previously. The incision site along the dorsal surface of the skin and the underlying musculature were reopened, and clamps from the IH impactor apparatus were attached to vertebra adjacent to the injury site (~T8 and T12) in order to immobilise the spinal column of the animal. Any scar tissue overlying the spinal cord was removed using fine forceps (Dumont #5 forceps; FST) and the dura carefully opened using a fine needle tip (26G; Terumo, Shibuya, Tokyo, Japan) without disturbing the spinal cord. Glass micropipettes (60 μm tip diameter; Blaubrand, Wertheim, Baden-Württemberg, Germany) for cell injection were pulled using a P-2000 Laser-Based Micropipette Puller (Sutter Instruments, Novato, CA, USA) with the following settings; heat = 750, filament = 5, velocity = 30, delay = 200, pull = 50. Fine forceps (FST) were used to modify the pipette tip to the appropriate diameter. The micropipette was attached to a 10 μL Hamilton syringe (Hamilton, Reno, NV, USA) with polyethylene tubing (Becton Dickinson, Franklin Lakes, NJ, USA) and positioned using a stereotaxic frame (Kopf Instruments; Tujunga, CA, USA). Two injections of 2.5 × $10^5$ donor hMSCs/nv-hMSCs in 4 μL PBS (5 × $10^5$ cells in 8 μL total) were delivered into the contusion site (rostral and caudal to the lesion epicentre, at the midline of the spinal cord) at a depth of 1 mm. Donor cells were delivered at a rate of 0.5 μL/min for 8 minutes using a syringe pump (Harvard Apparatus, Holliston, MA, USA). The micropipette was left in

place for 1 minute following delivery to minimize efflux of cells after pipette withdrawal. Following transplantation, muscles were again sutured and overlying skin closed with wound clips. Animals were returned to clean cages and placed in a heating cabinet (26°C) for 24 hours to aid recovery following surgery. Rehydrating normal saline, analgesic and antibiotic were administered for 1 week post-surgery, as described above (Hodgetts et al., 2013a, b, 2018).

**Functional analyses**

Functional recovery assessment in spinal cord injury studies require multiple tests in order to indicate robust outcomes. Whilst it is not always possible to link functional outputs directly to any morphological improvements or changes, a range of different functional outputs were used to assess; hindlimb (HL) recovery specifically in open field and on a horizontal ladder (as a general indicator of recovery of function with time). Additionally our own RatWalk gait analysis was used to reveal any potential changes in patterns of forelimb/hindlimb (FL/HL) coordination. HL function was assessed weekly using open field locomotor (BBB) scoring (Basso et al., 1995), LadderWalk, and RatWalk analyses.

***Open field locomotor analysis***

Hindlimb (HL) function was assessed weekly from day 7 post-SCI using the 21-point Basso, Beattie, Bresnahan (BBB) locomotor rating scale (Basso et al., 1995). Rats were allowed to freely move about an open field for 3–4 minutes while observers scored the degree of HL function demonstrated. At least two observers independently scored each animal and all observers were blinded to the treatment group. All BBB runs were video recorded for further analysis by additional observers (if needed). Individual scores were assigned for the right (R) and left (L) HL, and the highest recorded score was used for analysis (most scores differed by ≤ 2 points). BBB scores for each treatment at each time point were averaged and are presented as non-rounded values. Rats that attained a BBB score of 10, representing occasional (≤ 50%) weight supported plantar steps, were subjected to further behavioural testing on LadderWalk and RatWalk platforms.

***LadderWalk analysis***

Rats were video recorded while completing 3 passes of a 1 m long horizontal ladder with varying distances between the ladder rungs (Soblosky et al., 1997; Metz and Whishaw, 2002; Webb and Muir, 2003; Hodgetts et al., 2018). The number of right (R) and left (L) HL missteps were noted individually, where a misstep was defined as an incorrect paw placement that results in the foot falling below the ladder rungs and/or the loss of controlled HL weight support. The total number of missteps (R + L HL missteps) were averaged over the 3 passes for each animal and used to calculate the average number of missteps for each treatment group at each time point.

***RatWalk analysis***

Rats completed 3 passes across a 1-m long horizontal glass platform while their paw prints were video recorded from below. The paw prints were later identified and assigned as right or left (R/L) and fore- or hind-limb (FL/HL), in step sequence, using the RatWalk computer program designed independently in our laboratory (Godinho et al., 2013; Hodgetts et al., 2018), based on the CatWalk program (Hamers et al., 2001, 2006). RatWalk generates data that reflects locomotor characteristics such as step sequence, coordination pattern, stride length and stance width (Godinho et al., 2013; Hodgetts et al., 2018). The results generated were averaged over the 3 passes for each animal, then averaged for each treatment group at each time point.

**Tissue processing and morphological analysis**

Eight weeks after SCI, animals were euthanased with a lethal injection (IP) of sodium pentobarbitone (lethabarb; Virbac, Carros, France). A heart bleed was performed immediately before transcardial perfusion with 150 mL of heparinised PBS (1% (v/v) heparin, Hospira, Lake Forest, IL, USA) and fixation with 150 mL of 4% (w/v) PFA. The vertebral column was removed and post-fixed (4% (w/v) PFA) for at least 24 hours at 4°C before the spinal cord was dissected out and stored in 4% (w/v) PFA at 4°C.

A 1 cm segment of spinal cord, with the injury site at the midpoint of the segment, was removed for sectioning. Spinal cord segments were cryoprotected in 30% (w/v) sucrose in PBS overnight (O/N) at 4°C, then embedded in 10% (w/v) gelatin (Difco™; Becton Dickinson) in PBS. Blocks were fixed in 4% (w/v) PFA for 2 hours at RT, cryoprotected in 30% (w/v) sucrose O/N at 4°C, then frozen O/N at –20°C. Spinal cord blocks were sectioned using a CM3050 Leica cryostat (temperature maintained at –22°C to –20°C; Leica Biosystems, Nussloch, Baden-Württemberg, Germany) and serial 40 µm thick longitudinal sections were transferred in sequence to 24-well plates containing 0.2% (v/v) sodium azide (Sigma-Aldrich) in PBS. All sections were stored at 4°C until used for histological staining and immunohistochemistry.

**Toluidine blue staining and cyst analysis**

To analyze cyst formation within the lesion site, every sixth spinal cord section was mounted onto subbed slides (2% (w/v) gelatin, 0.2% (w/v) chromium (III) potassium sulphate (Sigma-Aldrich) in $dH_2O$) and allowed to air-dry O/N. Slides were submerged in toluidine blue solution (0.05% (w/v) Toluidine blue O (Sigma-Aldrich) and 0.005% (w/v) sodium tetraborate (Sigma-Aldrich) for 30–40 seconds, immediately rinsed in $dH_2O$ and dehydrated in graded alcohols (70, 90 and 100% (v/v)) for 3 minutes each. Slides were air-dried O/N then coverslipped with Leica CV Mount (Leica Biosystems).

Toluidine blue stained slides were scanned at 20X magnification using a Leica Aperio ScanScope XT digital slide scanner (Leica Biosystems), and the resulting data files were processed using Aperio ImageScope software (Leica Biosystems). Image-Pro Plus software (version 6.2; Media Cybernetics, Rockfield, MD, USA) was used to outline the borders of each section and all cysts, in order to calculate the total tissue and cyst areas. The cyst areas for each section were summed and used to calculate the total cyst area as a percentage of the total section area. The percentage cyst for each section was averaged across all sections analyzed to give the average percentage cyst per animal, which was then averaged for each treatment group (Hodgetts et al., 2013a, b, 2018).

**Immunohistochemistry and fluorescence quantitation**

The fluorescence intensity of neuronal [βIII tubulin, growth associated protein-43 (GAP43), SMI32], glial [S100, glial fibrillary acidic protein (GFAP)], extracellular matrix (ECM; laminin) and immune cell (Iba1, ED1) markers was analyzed on three sections (each 240–320 µm apart) per antibody, surrounding the midline of the spinal cord. Free-floating sections were blocked in 10% (v/v) FBS and 0.02% (v/v) Triton-X 100 in PBS for 30 minutes at RT. Sections were washed 3 times over 5 minutes in PBS and incubated with primary antibodies (**Table 2**) diluted in PBS O/N at 4°C in a humidified chamber. Primary antibodies were removed, sections were washed 3 times over 5 minutes in PBS and incubated with secondary antibodies (**Table 2**) diluted in PBS for 30 minutes at RT, protected from light. Secondary antibodies were then removed and sections washed 3 times over 5 minutes in PBS, mounted onto slides (Menzel-Gläser, ThermoFisher Scientific, Waltham, MA, USA) and allowed to air-dry (1–2 hours) before being coverslipped with ProLong® Diamond Antifade Mountant (Molecular Probes, Eugene, OR, USA) and air-dried O/N, protected from light. All slides were stored at 4°C and protected from light until imaged.

Tiled fluorescent images were taken at 20× magnification using a Photometrics CoolSNAP EZ camera (Teledyne Photometrics, Tucson, AZ, USA) attached to a Nikon Eclipse Ti microscope (Coherent Scientific, Australia) with NIS-Elements BasicResearch software (Melville, NY, USA). For analysis of fluorescence intensity (used as an indicator of the amount of protein expression), the images for each antigen were taken using the same exposure time, gain and camera settings. Sections were not exposed to light prior to imaging and all sections stained with a particular antibody, for each experiment, were imaged on the same platform during the same imaging session. Images were analyzed with NIS-Elements BasicResearch software to determine the fluorescence intensity of whole images. The threshold for fluorescence intensity was set/determined using secondary only (negative/secondary control) stained sections to assign background fluorescence. Pixels above background were counted as positive and the amount of positive fluorescence per field of view was recorded. The minimum, maximum, average and sum intensity were recorded and averaged across the 3 images for each animal, then averaged for each treatment group.

### Detection and quantification of human nuclei

Human MPC survival was confirmed with human nuclear antigen (HNA) STEM101 antibody to detect human nuclei in Nude rat spinal cord sections. The *in vivo* presence of donor hMSCs and possible interactions between the cell graft and host tissue were assessed with double labelling of STEM101 with various markers, and also by immunostaining sections adjacent to those containing STEM101 positive cells. Three sections per animal were double stained to compare the distribution of STEM101$^+$ cells with βIII tubulin (neuronal), GFAP (glial), and laminin (ECM) immunoreactivity. Sections analyzed were selected based on the results of toluidine blue staining. For identification of human nuclei (hMSCs), tiled confocal images were taken at 20× magnification on a Nikon A1 Confocal Microscope (Nikon) (Coherent Scientific, Australia) with NIS-Elements AdvancedResearch software (version 4.13; Nikon, Melville, NY, USA). Images were taken at 1.5 µm z-step intervals through the tissue, and the resulting image at each step was analyzed for antigen co-localisation. Maximum intensity projection images were created from z-stacks using NIS-Elements AdvancedResearch software. Due to limitations on the location of sections (within the spinal cord and relative to the cell transplant location) and the number of sections available for STEM101 immunohistochemistry, one section per animal was used for human nuclei counts. The section that appeared to have the largest number of STEM101$^+$ nuclei was analyzed. STEM101$^+$ human nuclei were manually counted using Image-Pro Plus software (Media Cybernetics, Rockville, MD, USA) and the average number of human nuclei calculated for each treatment group.

### Statistical analysis

Statistical tests were conducted using GraphPad Prism (version 7.01; GraphPad, San Diego, CA, USA) and/or GenStat (18$^{th}$ Edition; VSN International Ltd., Hemel Hempsted, Hertfordshire, UK). Statistical analysis of BBB scoring was carried out using the Kruskal-Wallis test (non-parametric analysis of variance (ANOVA)) with Bonferroni correction for multiple comparisons. One- or two-way ANOVA with Fisher's least significant difference (LSD; at 5%) were used for all other analyses to assess differences between pre-injury animals and each treatment group (one-way), and differences between treatment groups (two-way). We considered statistical significance at $P < 0.05$. Quantitative analysis of donor hMSC survival at 7 weeks post-transplantation (**Table 3**) was performed using a two-sample *t*-test.

**Table 3 | Quantitative analysis of donor hMSC survival at 7 weeks post-transplantation**

| Treatment | Samples with hMSCs Identified | | Average # STEM101 nuclei (mean ± SEM) |
|---|---|---|---|
| | Toluidine Blue | STEM101$^+$ nuclei | |
| hMSCs | 83% (5/6) | 100% (4/4) | 221.8±30.5$^{*\#}$ |
| mAPP96-110 + hMSCs | 100% (4/4) | 100% (4/4) | 342±153.8 |
| APP96-110 + hMSCs | 88% (7/8) | 100% (4/4) | 118.8±13.9$^{*}$ |
| nv-hMSCs | 0% (0/7) | 0% (0/4) | 0±0 |
| APP96-110 + nv-hMSCs | 0% (0/8) | 0% (0/4) | 0±0 |

Toluidine blue staining and STEM101 immunofluorescence indicated that only viable hMSCs survived to 7 weeks post-transplantation. There was a significant increase in the number of STEM101$^+$ human nuclei with viable hMSCs (hMSCs, APP96-110 + hMSCs) *vs.* nv-hMSCs (nv-hMSCs, APP96-110 + nv-hMSCs) (*), and with hMSCs *vs.* APP96-110 + hMSCs (#$P < 0.05$, two-sample *t*-test). APP96-110: Amyloid precursor protein peptide; hMSCs: human mesenchymal stromal cells; mAPP96-100: mutant amyloid precursor protein; nv: non-viable.

## Results

### Functional recovery

After the complete loss of HL function immediately following SCI (D0) there was a gradual recovery of function over the 8 week experimental period (**Figure 1**). However, while the nv-hMSC group consistently showed the lowest BBB scores, statistical analysis did not reveal any significant differences in the functional recovery between SCI only and any treatment group, nor between groups, for any functional test up to D56. No group recovered to pre-injury scores. There was a significant increase in BBB score with APP96-110 + nv-hMSCs compared to nv-hMSCs at D49 ($P < 0.05$; **Figure 1**), however this was not maintained for the following (final) week. By D56, all groups demonstrated occasional to frequent weight-supported plantar stepping (BBB 10 to 11) with no significant differences in the average BBB score between any groups at D56 (**Figure 1**; $P > 0.05$).

LadderWalk analysis showed a significant impact of SCI on HL function (**Figure 2**), as seen by a significant increase in the number of missteps at D35 (A) and D56 (B) post-SCI compared to pre-injury scores ($P < 0.05$). While no group recovered to pre-injury scores, there were significantly fewer missteps at D35 for SCI only, hMSCs and APP96-110 + nv-hMSCs compared to nv-hMSCs ($P < 0.05$), and at D56 for mAPP96-110 and APP96-110 compared to mAPP96-110 + hMSCs ($P < 0.05$).

RatWalk analysis was used to assess aspects of functional recovery such as stance width, stride length and the frequency of different coordinating patterns for animals that had attained a BBB score of 10, demonstrating occasional weight-supported plantar stepping. SCI significantly reduced forelimb (FL) and HL stance widths and stride lengths at D35 and D56 compared to pre-injury ($P < 0.05$, one-way ANOVA). FL stance width and stride lengths were 42–50% shorter, and HL stance width and stride lengths were 18–28% shorter post-injury compared to pre-injury. There were largely no differences in stance width or stride length between treatments; however at D56, HL stride lengths were larger (~20%) for SCI only, APP96-110 and nv-hMSCs compared to hMSCs (data not shown; $P < 0.05$, two-way ANOVA significance for HL). Importantly, there were no progressive differences in stance width or stride length for each treatment between D35 and D56, indicating no consistent change or improvement with time. With regard to coordinating patterns of limb movement, there were no significant differences in the amount of each coordinating pattern demonstrated pre-injury compared to D35 and D56 post-SCI (data not shown). This is possibly due to the large variation in the amounts of each coordinating pattern demonstrated by individual animals during triplicate RatWalk passes (pre- and post-injury), and the likelihood that animals

will use some coordinating pattern to locomote (once weight supported stepping has returned) regardless of injury severity or amount of HL functional control.

**Morphological and immunohistochemical analyses**

***APP96-110 peptide combined with MSC transplants***

Areas with grafted hMSCs appeared in toluidine blue stained sections as dark blue stained, dense, fibrous areas that had a particular alignment within the tissue (extending rostral/caudal from the injection site or dorsal/ventral along the transplantation needle track – data not shown). Neuronal marker profiling identified a clear injury site that was void of organized neuronal tissue, lacked distinguishable grey and white matter regions and was bordered rostrally and caudally by uninjured tissue, and ventrally by spared tissue. In some cases, the injury site extended up to 6 mm in length (rostral/caudal). The number of βIII tubulin$^+$, GAP43$^+$ and SMI32$^+$ fibers varied greatly between groups and appeared to be denser and more numerous in hMSC treated animals. The majority of neuronal fibers extending within the lesion site lacked specific orientation and organization, however many fibers were orientated with the hMSC graft in hMSC treated animals. At D56 (49 days post-transplantation) numerous βIII tubulin$^+$ axons filled the lesion site and were closely associated with STEM101$^+$ hMSCs (**Figure 3A1** and **B1**). Similarly, numerous GAP43$^+$ (**Figure 3A2** and **B2**) and SMI32$^+$ (**Figure 3A3** and **B3**) fibers surrounded and extended through hMSC graft areas. Neuronal fibers appeared to be denser and more aligned when associated with hMSC graft areas, perhaps indicating that the grafted cells promoted and/or supported the regrowth/regeneration of neuronal processes.

STEM101 distinguishes uniformly sized, oval human nuclei from surrounding autofluorescent macrophages (intense,varied autofluorescence and a foamy/spongy morphology with uneven borders). Human MSCs often migrated 1–3 mm (rostral/caudal) within the lesion site itself and in some cases extended dorsal/ventral within the needle track (data not shown). Viable STEM101$^+$ donor hMSCs survived to at least 7 weeks after transplantation (**Table 3**). However, even at 7 weeks post-transplantation there was no evidence of migration of viable hMSCs into adjacent intact host tissue. There was a significant increase in the average number of STEM101$^+$ nuclei with viable hMSCs (hMSCs only and APP96-110 + hMSCs) compared to nv-hMSCs (nv-hMSCs only and APP96-110 + nv-hMSCs; $P < 0.05$). There was also a significant increase in the average number of STEM101$^+$ nuclei with hMSCs compared to APP96-110 + hMSCs ($P < 0.05$), however neither group was significantly different to mAPP96-110 + hMSCs ($P > 0.05$), due to the large variance in STEM101$^+$ human nuclei counts of mAPP96-110 + hMSCs animals.

Astrocytes (S100$^+$ or GFAP$^+$) were evenly distributed throughout uninjured tissue and present within the lesion site to varying degrees. The lesion site was largely devoid of S100 and GFAP immunoreactivity, particularly in cell transplanted animals. GFAP immunoreactivity was strongest in tissue immediately adjacent to the injury site and/or hMSC graft regions. There was limited interaction between donor hMSCs and host glial cells, identified by GFAP (astrocytes) or S100 (astrocytes and perhaps infiltrating Schwann cells) immunoreactivity. As shown in **Figure 4A1** and **B1**, there was intense GFAP immunoreactivity at the border between host tissue and the hMSC graft with very few GFAP$^+$ processed extending into the graft. S100 immunoreactivity followed a similar pattern with abundant S100$^+$ profiles surrounding the graft and few S100$^+$ process extending into the graft area (not shown).

Laminin deposits filled and bridged the lesion site of all animals, extending between uninjured rostral and caudal tissue. Extensive tubular laminin deposits filled the lesion site of all hMSC transplanted animals and appeared to be greatest in areas within and immediately surrounding the hMSC graft (not quantified; **Figure 4A2** and **B2**). Accordingly, laminin$^+$ profiles were often orientated with the direction of the hMSC graft.

Iba1$^+$ and ED1$^+$ microglia/macrophages were present within the lesion site and in surrounding uninjured tissue of all animals at 8 weeks post-SCI. Iba1 and ED1 immunoreactivity identified resident and infiltrating microglia/macrophages within the injury site that had either an amoeboid morphology with short processes characteristic of activated microglia or a large, foamy/spongy morphology characteristic of phagocytotic microglia/macrophages (ED1$^+$, **Figure 4A3** and **B3**). Iba1$^+$ cells present within the injury site often aligned with the hMSC graft while ED1$^+$ cells were often concentrated at the border of the graft with few ED1$^+$ cells infiltrating the graft area. ED1 immunoreactivity appeared weaker within graft areas than the surrounding tissue, suggesting that donor hMSCs may be influencing the activation and infiltration of microglia/macrophages to varying degrees.

Every sixth spinal cord section was toluidine blue stained to visualise tissue morphology and cyst formation. Cyst formation occurred in all animals following SCI. Large cysts were visible within the lesion epicentre of SCI only and APP96-110 treated animals, and in some cases, some cyst formation occurred in tissue rostral and caudal to the lesion site. In contrast, in animals that also received cell grafts, spared/sprouting/regrowing tissue and extracellular matrix (ECM) deposits were present within the lesion epicentre, with numerous smaller cysts surrounding the lesion site, and in tissue rostral and caudal to the lesion site (data not shown). After quantifying these cyst sizes, it was revealed that treatment with mAPP96-110 significantly reduced cyst size (**Figure 5**) compared to SCI only ($P < 0.05$), while combined treatment with mAPP96-110 + hMSCs, APP96-110 + hMSCs and APP96-110 + nv-hMSCs significantly reduced cyst size compared to SCI only and APP96-110 ($P < 0.05$). APP96-110 + hMSCs also significantly reduced cyst size compared to nv-hMSCs ($P < 0.05$).

**Quantification of immunostaining**

***Neuronal markers***

There was a significant increase in the average fluorescence intensity of βIII tubulin with hMSCs, mAPP96-110 + hMSCs, APP96-110 + hMSCs and APP96-110 + nv-hMSCs compared to SCI only, mAPP96-110 and APP96-110 and nv-hMSCs ($P < 0.05$, two-way ANOVA). There was also a significant increase with nv-hMSCs compared to SCI only (**Figure 6A**). Conversely, there was a significant decrease in the average fluorescence intensity of SMI32 with hMSCs, APP96-110 + hMSCs, nv-hMSCs and APP96-110 + nv-hMSCs compared to SCI only, mAPP96-110 and APP96-110, and mAPP96-110 + hMSCs compared to mAPP96-110 and APP96-110, and a significant increase in SMI32 fluorescence intensity with mAPP96-110 and APP96-110 compared to all other groups (no difference between mAPP96-110 and APP96-110) ($P < 0.05$, two-way ANOVA) (**Figure 6C**). There was no difference in the average fluorescence intensity of GAP43 between any groups ($P > 0.05$, two-way ANOVA) (**Figure 6B**).

***Glial markers***

There was a significant decrease in the average fluorescence intensity of S100 with APP96-110 + hMSCs and nv-hMSCs compared to mAPP96-110 and/or APP96-110 ($P < 0.05$, two-way ANOVA). Whereas mAPP96-110 and APP96-110 significantly increased S100 fluorescence intensity compared to SCI only (**Figure 6D**). There was a significant increase in the average fluorescence intensity of GFAP with hMSCs, mAPP96-110 + hMSCs, APP96-110 + hMSCs and APP96-110 + nv-hMSCs compared to SCI only, mAPP96-110 and APP96-110,

and with nv-hMSCs compared to SCI only and mAPP96-110 ($P$ < 0.05, two-way ANOVA) (**Figure 6E**).

### *Laminin*

There was a significant increase in the average fluorescence intensity of laminin with APP96-110, hMSCs, APP96-110 + hMSCs and nv-hMSCs compared to SCI only and/or mAPP96-110, and mAPP96-110 + hMSCs and APP96-110 + nv-hMSCs compared to SCI only, mAPP96-110 and APP96-110, and/or hMSCs ($P$ < 0.05, two-way ANOVA) (**Figure 6F**).

### *Microglia/macrophage markers*

There was no difference in the average fluorescence intensity of Iba1 between any groups ($P$ > 0.05, two-way ANOVA) (**Figure 6G**), however there was a significant decrease in the fluorescence intensity of ED1 with hMSCs, APP96-110 + hMSCs, nv-hMSCs and APP96-110 + nv-hMSCs compared to mAPP96-110 and APP96-110 ($P$ < 0.05, two-way ANOVA) (**Figure 6H**).

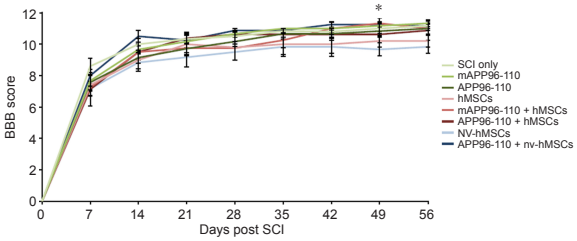


**Figure 1 | Open field locomotor recovery as assessed with BBB scoring.**
Weekly average BBB scores (± SEM) show a gradual recovery of hindlimb function following induction of SCI at D0. At D49, APP96-110 + nv-hMSCs (dark blue) scored significantly higher than nv-hMSCs (light blue) (*$P$ < 0.05, Kruskal-Wallis test). There were no significant differences in average BBB score at D56 between any groups, with hMSCs and nv-hMSCs attaining a rounded average BBB score of 10, and all other groups attaining a rounded average BBB score of 11 ($P$ > 0.05, Kruskal-Wallis test). Uninjured animals score 21. Data are expressed as the mean ± SD. Numbers of animals ($n$ = 4–8) for each treatment group are shown in Table 1. APP96-110: Amyloid precursor protein peptide; BBB: Basso, Beattie, Bresnahan locomotor rating scale; hMSCs: human mesenchymal stromal cells; mAPP96-100: mutant amyloid precursor protein; nv: non-viable; SCI: spinal cord injury.

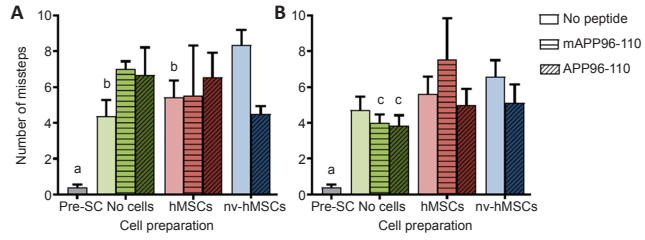


**Figure 2 | Hindlimb functional recovery as assessed by LadderWalk.**
There was a significant increase in the average number of missteps (± SEM) post-spinal cord injury (all coloured bars) compared to pre-injury (grey bar) see "a" ($P$ < 0.05, one-way analysis of variance followed by Fisher's least significant difference test). At D35 (A), spinal cord injury only (no cells), hMSCs, and APP96-110 + nv-hMSCs groups exhibited significantly fewer missteps (see "b") than nv-hMSCs (light blue) ($P$ < 0.05, two-way ANOVA followed by Fisher's least significant difference test). At D56 (B), mAPP96-110 and APP96-110 exhibited significantly fewer missteps than mAPP96-110 + hMSCs (medium red) (see "c") ($P$ < 0.05, two-way ANOVA followed by Fisher's least significant difference test). In the mAPP96-110 treatment group there was a significant reduction in the average number of missteps from D35 to D56 ($P$ < 0.05, two-sample $t$-test). No group recovered to pre-injury scores ($P$ > 0.05, two-way ANOVA followed by Fisher's least significant difference test). Open bars indicate no peptide, horizontal striped bars indicate mAPP96-110 treatment, diagonal striped bars indicate APP96-110 treatment. Data are expressed as the mean ± SD. Numbers of animals ($n$ = 4–8) for each treatment group are shown in Table 1. ANOVA: Analysis of variance; APP96-110: amyloid precursor protein peptide; hMSCs: human mesenchymal stromal cells; mAPP96-100: mutant amyloid precursor protein; nv: non-viable.

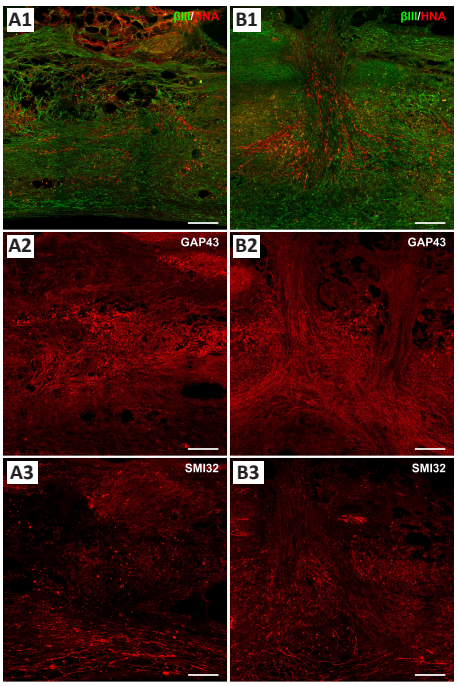


**Figure 3 | Immunostaining of adjacent longitudinal sections of the same injured spinal cord grafted with donor hMSCs, examined at D56 (49 days post-transplantation) revealing neuronal marker (βIII tubulin$^+$, GAP43$^+$ and SMI32$^+$ fiber) profiles in injury sites.**
Neuronal marker (βIII tubulin$^+$, GAP43$^+$ and SMI32$^+$ fiber) profiles in injury sites appeared to be denser and more numerous in hMSC treated animals, but lacked specific orientation and organization. STEM101 marker (HNA, red) co-stained with βIII tubulin$^+$ (green) axons that fill the lesion site (A1, B1); numerous GAP43$^+$ (red; A2, B2) and SMI32 fibers (red; A3, B3) surrounded and extended through hMSC graft areas. Scale bars: 200 µm. GAP43: growth associated protein-43; hMSCs: human mesenchymal stromal cells; HNA: human nuclear antigen.

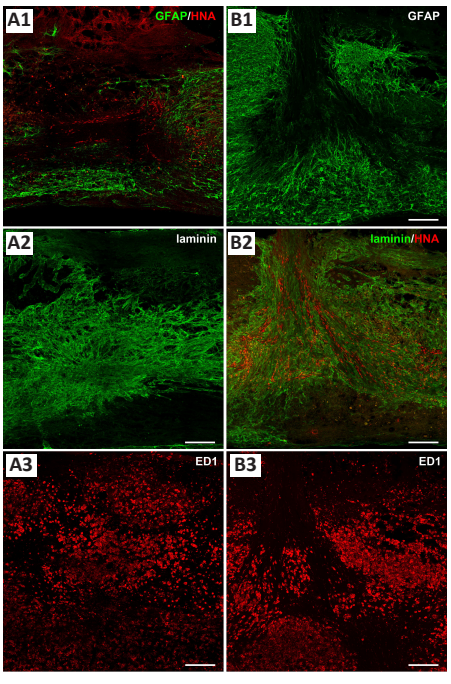


**Figure 4 | Immunostaining of adjacent longitudinal sections of the same injured spinal cord grafted with donor hMSCs examined at D56 (49 days post-transplantation) revealing astrocytic (GFAP$^+$), extracellular matrix (laminin$^+$) and microglial/macrophage (ED1$^+$) marker profiles in injury sites.**
Intense GFAP immunoreactivity restricted at the hMSC graft border had very few GFAP$^+$ processes extending into the graft, whilst laminin deposits and ED1$^+$ cells often filled and bridged the lesion site, extending between uninjured rostral and caudal tissue. STEM101 marker (HNA; red) co-stained with GFAP (green; A1, B1), laminin (green; A2, B2) and ED1 (red; A3, B3) throughout hMSC graft areas. Scale bars: 200 µm. GFAP: Glial fibrillary acidic protein; hMSCs: human mesenchymal stromal cells; HNA: human nuclear antigen.

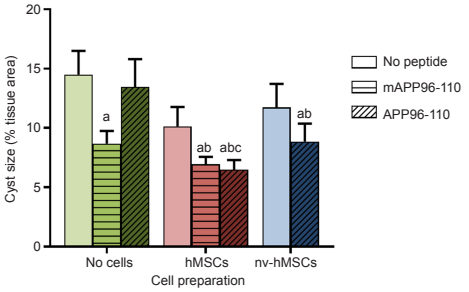


**Figure 5** | **Cyst size quantification from toluidine blue stained sections analyzed at 8 weeks post SCI.**

Treatment with mAPP96-110 significantly reduced cyst size compared to SCI only ("no cells") (a), while combined treatment with mAPP96-110 + hMSCs, APP96-110 + hMSCs and APP96-110 + nv-hMSCs significantly reduced cyst size compared to SCI only and APP96-110 (b). APP96-110 + hMSCs also significantly reduced cyst size compared to nv-hMSCs (c) ($P < 0.05$, two-way analysis of variance followed by Fisher's least significant difference test). Data are expressed as the mean ±SD. Numbers of animals ($n = 4–8$) for each treatment group are shown in Table 1. APP96-110: Amyloid precursor protein peptide; hMSCs: human mesenchymal stromal cells; mAPP96-100: mutant amyloid precursor protein; nv: non-viable; SCI: spinal cord injury.

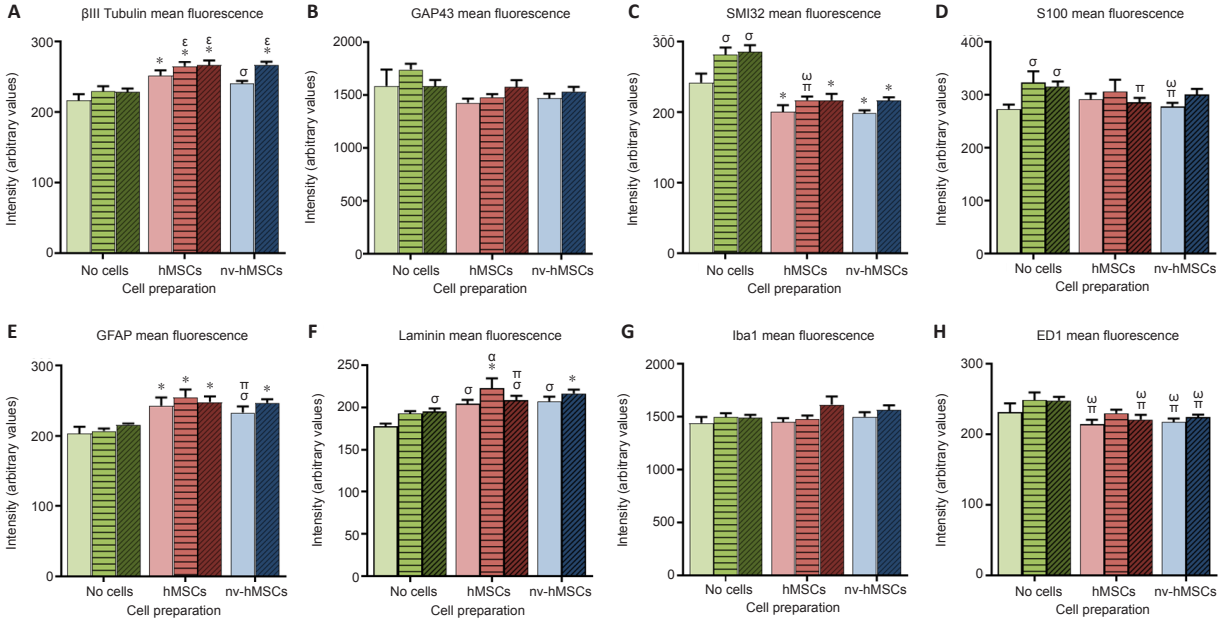


**Figure 6** | **Mean fluorescence intensities of various immunostained sections.**

Cell transplantation (hMSCs, red bars; nv-hMSCs, blue bars) affected fluorescence intensity more than treatment with mAPP96-110 (± viable/nv-hMSCs; horizontal striped bars) or APP96-110 (± viable/nv-hMSCs; diagonal striped bars). Cell transplantation significantly increased the mean fluorescence intensity of βIII tubulin (A), GFAP (E) and laminin (F), decreased SMI32 (C), S100 (D; APP96-110 + hMSCs and nv-hMSCs only) and ED1 (H), and had no effect on GAP43 (B) or Iba1 (G) fluorescence intensity. mAPP96-110 and APP96-110 significantly increased the mean fluorescence intensity of SMI32 (C), S100 (D) and laminin (F; APP96-110 only). Significance to SCI, mAPP, APP (*), SCI (σ), mAPP96-110 (π), APP96-110 (ω), hMSCs (α) and nv-hMSCs (ε); ($P < 0.05$, two-way analysis of variance followed by Fisher's least significant difference test). Data are expressed as the mean ± SEM. APP96-110: Amyloid precursor protein peptide; GAP43: growth associated protein-43; GFAP: glial fibrillary acidic protein; hMSCs: human mesenchymal stromal cells; mAPP96-100: mutant amyloid precursor protein; nv: non-viable.

## Discussion

Based on recent studies reporting neuroprotective effects of APP96-110 following TBI (Corrigan et al., 2014; Plummer et al., 2016, 2018), we investigated the neuroprotective potential of the APP96-110 peptide following SCI. In summary, while occasional functional improvements were seen, they were inconsistent between groups and across BBB, LadderWalk and Ratwalk tests, thus their biological significance is unconvincing. Nonetheless, there were some improvements in outcomes using morphological measures. Surprisingly, and for reasons that remain unclear, the mutant APP96-110 peptide, but not APP96-110, significantly reduced cyst size compared to SCI. Importantly however, both peptides significantly reduced cyst size when combined with viable hMSCs, an effect that was not seen with hMSC transplantation alone. In our previous studies treatment with human mesenchymal precursor cells after SCI resulted in reduced cyst size (Hodgetts et al., 2013a, b), which may highlight the possibility of specific donor variation within these human mesenchymal isolates. Fluorescence intensity was used as an indicator of the amount of protein expression for each antigen in spinal cord sections. Treatments with viable and nv hMSC transplantation (± APP96-110) significantly increased βIII tubulin, GFAP and laminin, and decreased SMI32, S100 and ED1 fluorescence intensity, whereas mAPP96-110 and APP96-110 alone significantly increased SMI32 and S100 fluorescence intensity. Donor hMSC survival was significantly higher with hMSCs compared to APP96-110 + hMSCs, however neither group differed when compared to mAPP96-110 + hMSCs.

Importantly, the same peptides and essentially identical protocols/doses used in the previous brain studies (Corrigan et al., 2014; Plummer et al., 2016, 2018) were used in our SCI model, and yet resulted in different outcomes from a functional perspective. We consider below how the potential factors defining the efficacy of a particular therapeutic approach in one CNS injury model may not necessarily be observed in other neurotrauma models.

Administered alone, APP96-110 peptide did not produce any consistent improvements in either functional or morphological outcomes post-SCI. While the effectiveness of a therapeutic approach in a particular CNS injury model often provides the justification for investigation in other models, it does not guarantee that similar outcomes will occur. It seems likely that the neuroprotective effects of APP96-110 following TBI reported previously by Corrigan et al. (2014) and Plummer et al. (2018) were not replicated in this study due to differences in the animal and CNS injury models used. Not only are there significant differences in the inflammatory response (and injury development in SCI) between mice and rats (Sroga et al.,

2003), but also between different strains of the same species (Popovich et al., 1997; Kigerl et al., 2006), and between animals of different ages (Kumamaru et al., 2012; Sutherland et al., 2016). Although both are part of the CNS, the brain and spinal cord exhibit significantly different inflammatory immune responses [reviewed by Zhang and Gensel (2014)]. Overall, the timing and duration, and magnitude of the inflammatory immune response to injury is greater in the spinal cord than the brain, with significantly greater microglia/macrophage and astrocyte activation, and neutrophil and lymphocyte infiltration following SCI than TBI (Schnell et al., 1999; Batchelor et al., 2008). Injury severity also significantly affects the magnitude of the inflammatory response with the amounts of blood-spinal cord barrier (BSCB) and inflammatory tissue damage, and secondary degeneration directly related to the force of the primary mechanical injury (Noble and Wrathall, 1989a, b; Yang et al., 2005; Maikos and Shreiber, 2007). Consequently, some pharmacological and cell-based therapies that are efficacious in mild SCI are less effective in moderate or severe injury models [e.g. cell transplantation (Himes et al., 2006; Zheng et al., 2011; Yokota et al., 2015)]. Clearly then, potential neuroprotective therapies for CNS trauma need to be tailored to suit the injury model and injury severity accordingly.

The dose and route of administration can also affect the efficacy of pharmacological therapies. Increasing the concentration of APP96-110 significantly improves neuroprotective effects following TBI, possibly due to increased heparin binding (from more peptide being available) leading to increased downstream effects that contribute to greater neuroprotection. Because of this, and the differences in the inflammatory immune responses between TBI and SCI discussed previously, future studies should investigate the effects of increased APP96-110 concentrations following SCI, in order to determine whether APP96-110 can have neuroprotective effects following SCI, and whether these effects are dose dependent. Both intravenous and intracerebroventricular APP96-110 injections have been tested following TBI (Corrigan et al., 2014; Plummer et al., 2018). The latter approach bypasses the blood-brain barrier and delivers the peptide directly to the brain. Although intravenous injection may be less invasive and a more clinically relevant method of delivery than intraspinal injection, it relies on the peptide being able to cross the compromised BSCB or the peptide having systemic effects within the body. Although BSCB permeability is increased for a number of weeks following mechanical injury (Popovich et al., 1996), the overall permeability, and permeability to proteins of different molecular weights varies greatly with injury severity (Noble and Wrathall, 1989a, b; Maikos and Shreiber, 2007). It may be that direct injection into the spinal cord via intralesional or intrathecal injection (single administration), or implantation of a mini-osmotic pump (continuous administration) at the lesion site bypasses the BSCB and provides a more effective route of administration. The incorporation/fusion of neuroprotective peptides with nanoparticles, magnetic particles or other cell penetrating peptides (e.g. TAT) that can cross the BSCB may also improve peptide delivery to the spinal cord (Hwang and Kim, 2014; Busquets et al., 2015; McGowan et al., 2015; Funnell et al., 2019; Naqvi et al., 2020).

APP96-110 has been suggested to act via heparin binding due to its homology with the D1 heparin binding domain of APP (Corrigan et al., 2011, 2014), and the role of heparin sulphate proteoglycans (HSPGs) in neuronal development, synaptogenesis, cell survival, proliferation and neurite outgrowth (Cui et al., 2013; Swarup et al., 2013; Beller and Snow, 2014). Alternatively, HSPG-mediated peptide endocytosis may produce neuroprotective effects by modulating ion channels and cell surface receptors expressed on neurons (Amand et al., 2012; Meloni et al., 2015a, b). Poly-arginine/arginine-rich peptides exert neuroprotective effects on neurons *in vitro* by reducing calcium influx and subsequent calcium-mediated excitotoxicity, however these neuroprotective effects are inhibited if neuronal cultures are treated with heparin prior to peptide administration (Meloni et al., 2015b). Calcium influx inhibition is influenced by peptide cationic charge and arginine content (Meloni et al., 2015a, 2017). Despite being considered as neuroprotective, the modest inhibitory action of COG1410 and APP96-110 peptides in reducing excitotoxic neuronal calcium influx could be due to their relatively low cationic charge and the presence of only two arginine residues, compared to cationic arginine-rich peptides such as R18 (Chiu et al., 2017). Indeed, a recent study demonstrated that the cationic arginine-rich peptide R18 is more effective than either COG1410 or APP96-110 at reducing neuronal death and calcium influx following *in vitro* excitotoxicity, and that R18 showed greater efficacy than APP96-110 in reducing axonal injury and improving some functional outcomes after TBI (Chiu et al., 2017).

Treatment with arginine-rich peptides also significantly reduces expression of the N-methyl-D-aspartate (NMDA) receptor subunit NR2B (MacDougall et al., 2017) and it is hypothesised that HSPG-mediated peptide endocytosis (initiated by poly-arginine/arginine-rich peptide binding to HSPGs) also leads to the endocytosis of cell surface receptors that may be key mediators of neuronal excitotoxicity (Meloni et al., 2015b; MacDougall et al., 2017). Because APP96-110 is a short peptide (15 amino acids) with two arginine residues, it is considered to be an arginine-rich peptide and some of its neuroprotective effects may be mediated via HSPG-mediated endocytosis. It has been reported that the neuroprotective potential of APP96-110 in the brain is reduced when the APP96-110 peptide is modified to have reduced heparin binding ability ("mAPP96-110" in the present study) (Corrigan et al., 2014), and is increased (to a certain extent) with increased heparin binding ability (Plummer et al., 2016). We used the same heparin-binding peptides, shown to remain stable in the brain for at least 5 hours post injection (Van Den Heuvel, unpublished observations), in our SCI model. Interestingly, our new data showing a reduction in cyst size with the mutant APP96-110 peptide but not APP96-110 treatment suggests that heparin binding ability and HSPG-mediated neuroprotection may not completely account for our observations in the spinal cord after trauma.

APP96-110 is also likely to interact with the amyloid precursor-like protein 2 (APLP2), which is homologous with APP, expressed ubiquitously throughout the body (Aydin et al., 2012) and has roles in neuronal development, synaptogenesis, and synaptic plasticity and transmission (Wang et al., 2005; Weyer et al., 2011; Shariati et al., 2013). Like APP, APLP2 expression in the brain significantly increases following TBI (possibly accounting for the neuroprotective effects of APP96-110), however there are no reports on its expression in the spinal cord before or after injury. As APLP2 may be involved in mediating the neuroprotective effects of APP96-110, it is pertinent to determine APLP2 expression in uninjured *vs.* injured spinal cords. This study aimed to investigate the potential effects of APP96-110 on donor hMSC survival following transplantation, and whether reduced secondary degeneration (via neuroprotection) promotes a less inflammatory injury site environment that is more conducive to donor cell survival. On the contrary, the number of human nuclei present within the spinal cord at 7 weeks post-transplantation was significantly lower with APP96-110 + hMSCs compared to hMSCs only, however neither of these groups differed from mAPP96-110 + hMSCs. Due to the need for multiple immunohistochemistry runs only a limited number of sections were specifically available for analysis of hMSC survival; further studies will be therefore be needed to confirm these initial observations.

In summary, in contrast to previous neurotrauma studies in the brain, intravenous delivery of APP96-110 at the time of SCI did not produce comprehensive neuroprotective effects (Corrigan et al., 2014; Plummer et al., 2018); this may be associated with differences in the magnitude and development of inflammatory immune responses in TBI versus SCI (Schnell et al., 1999; Batchelor et al., 2008; Zhang and Gensel, 2014). Future studies investigating the effects of increased APP96-110 concentration, alternative routes of delivery, and increased heparin binding ability of APP96-110, may determine whether APP96-110 can indeed exert similar neuroprotective effects following SCI, and whether these neuroprotective effects can be enhanced. In a recent TBI study, animals treated with 0.05 or 0.5 mg/kg APP96-110 after 0.5 hours demonstrated significant improvements in motor outcome, with reduced axonal injury and neuroinflammation at 3 days post-TBI, whereas 5 μg/kg APP96-110 had no effect. In contrast, treatment with 5 μg/kg or 0.5 mg/kg APP96-110 at 5 hours post-TBI demonstrated significant improvements in motor outcome over 3 days, and a reduction in axonal injury (Plummer et al., 2018). Additional dose response and clinically relevant therapeutic time window studies are required to further evaluate the potential of the APP96-110 analogue as a neuroprotective therapy for SCI, and this is a current avenue of investigation. Even though we occasionally obtained beneficial events using the mutant APP96-110, it is hypothesised that active APP96-110 exerts its effects via heparin binding, and potentially the modification of cell surface ion channels and receptors thereby preventing neuronal excitotoxicity (Meloni et al., 2015b; MacDougall et al., 2017). Combining this approach with other neuroprotective therapies or approaches aimed at promoting spinal cord repair (e.g. cell transplantation, scaffolds, growth/trophic factors) may significantly enhance the effects of individual therapies and lead to greater functional and morphological improvements following injury.

**Author contributions:** *Experimental design, performed and provided training in surgical procedures, animal recovery and monitoring, behavioural assays, analysis of results, and primary author manuscript preparation: SIH. Performed surgical procedures, animal recovery and monitoring, behavioural assays, tissue processing: SJL, DBH, AF. Isolation and provision of clinical grade hMSCs for implantation: MS. Generation, purification and supply of APP96-110 and mAPP96-110 peptides, assistance with manuscript preparation: CVH. Assistance with experimental design, analysis of results and manuscript preparation: ARH. All authors approved the final version of the manuscript.*
**Conflicts of interest:** *The authors declare that they have no competing interests.*
*Editor note: ARH is an Editorial Board member of Neural Regeneration Research. He was blinded from reviewing or making decisions on the manuscript. The article was subject to the journal's standard procedures, with peer review handled independently of this Editorial Board member and their research groups.*
**Financial support:** *This work was supported by the Neurotrauma Research Program of Western Australia.*
**Institutional review board statement:** *All performed procedures were approved by The University of Western Australia Animal Ethics Committee (RA3/100/1460) on April 12, 2016.*
**Copyright license agreement:** *The Copyright License Agreement has been signed by all authors before publication.*
**Data sharing statement:** *Datasets analyzed during the current study are available from the corresponding author on reasonable request.*
**Plagiarism check:** *Checked twice by iThenticate.*
**Peer review:** *Externally peer reviewed.*


## References

Alexander JK, Popovich PG (2009) Neuroinflammation in spinal cord injury: therapeutic targets for neuroprotection and regeneration. Prog Brain Res 175:125-137.

Amand HL, Rydberg HA, Fornander LH, Lincoln P, Norden B, Esbjorner EK (2012) Cell surface binding and uptake of arginine- and lysine-rich penetratin peptides in absence and presence of proteoglycans. Biochim Biophys Acta 1818:2669-2678.

Aydin D, Weyer SW, Muller UC (2012) Functions of the APP gene family in the nervous system: insights from mouse models. Exp Brain Res 217:423-434.

Basso DM, Beattie MS, Bresnahan JC (1995) A sensitive and reliable locomotor rating scale for open field testing in rats. J Neurotrauma 12:1-21.

Batchelor PE, Tan S, Wills TE, Porritt MJ, Howells DW (2008) Comparison of inflammation in the brain and spinal cord following mechanical injury. J Neurotrauma 25:1217-1225.

Beller JA, Snow DM (2014) Proteoglycans: road signs for neurite outgrowth. Neural Regen Res 9:343-355.

Bethea JR, Dietrich WD (2002) Targeting the host inflammatory response in traumatic spinal cord injury. Curr Opin Neurol 15:355-360.

Bowes AL, Yip PK (2014) Modulating inflammatory cell responses to spinal cord injury: all in good time. J Neurotrauma 31:1753-1766.

Busquets MA, Espargaro A, Sabate R, Estelrich J (2015) Magnetic nanoparticles cross the blood-brain barrier: when physics rises to a challenge. Nanomaterials (Basel) 5:2231-2248.

Cao F, Jiang Y, Wu Y, Zhong J, Liu J, Qin X, Chen L, Vitek MP, Li F, Xu L, Sun X (2016) Apolipoprotein E-mimetic COG1410 reduces acute vasogenic edema following traumatic brain injury. J Neurotrauma 33:175-182.

Chiu LS, Anderton RS, Cross JL, Clark VW, Edwards AB, Knuckey NW, Meloni BP (2017) Assessment of R18, COG1410, and APP96-110 in excitotoxicity and traumatic brain injury. Transl Neurosci 8:147-157.

Corrigan F, Pham CL, Vink R, Blumbergs PC, Masters CL, van den Heuvel C, Cappai R (2011) The neuroprotective domains of the amyloid precursor protein, in traumatic brain injury, are located in the two growth factor domains. Brain Res 1378:137-143.

Corrigan F, Thornton E, Roisman LC, Leonard AV, Vink R, Blumbergs PC, van den Heuvel C, Cappai R (2014) The neuroprotective activity of the amyloid precursor protein against traumatic brain injury is mediated via the heparin binding site in residues 96-110. J Neurochem 128:196-204.

Cui H, Freeman C, Jacobson GA, Small DH (2013) Proteoglycans in the central nervous system: role in development, neural repair, and Alzheimer's disease. IUBMB Life 65:108-120.

Edwards AB, Anderton RS, Knuckey NW, Meloni BP (2017) Characterisation of neuroprotective efficacy of modified poly-arginine-9 (R9) peptides using a neuronal glutamic acid excitotoxicity model. Mol Cell Biochem 426:75-85.

Funnell JL, Balouch B, Gilbert RJ (2019) Magnetic composite biomaterials for neural regeneration. Front Bioeng Biotechnol 7:179.

Godinho MJ, Teh L, Pollett MA, Goodman D, Hodgetts SI, Sweetman I, Walters M, Verhaagen J, Plant GW, Harvey AR (2013) Immunohistochemical, ultrastructural and functional analysis of axonal regeneration through peripheral nerve grafts containing Schwann cells expressing BDNF, CNTF or NT3. PLoS One 8:e69987.

Gronthos S, Zannettino AC, Hay SJ, Shi S, Graves SE, Kortesidis A, Simmons PJ (2003) Molecular and cellular characterisation of highly purified stromal stem cells derived from human bone marrow. J Cell Sci 116:1827-1835.

Hagg T, Oudega M (2006) Degenerative and spontaneous regenerative processes after spinal cord injury. J Neurotrauma 23:263-280.

Hausmann ON (2003) Post-traumatic inflammation following spinal cord injury. Spinal Cord 41:369-378.

Herrmann R, Sturm M, Shaw K, Purtill D, Cooney J, Wright M, Phillips M, Cannell P (2012) Mesenchymal stromal cell therapy for steroid-refractory acute and chronic graft versus host disease: a phase 1 study. Int J Hematol 95:182-188.

Herrmann RP, Sturm MJ (2014) Adult human mesenchymal stromal cells and the treatment of graft versus host disease. Stem Cells Cloning 7:45-52.

Himes BT, Neuhuber B, Coleman C, Kushner R, Swanger SA, Kopen GC, Wagner J, Shumsky JS, Fischer I (2006) Recovery of function following grafting of human bone marrow-derived stromal cells into the injured spinal cord. Neurorehabil Neural Repair 20:278-296.

Hoane MR, Pierce JL, Holland MA, Birky ND, Dang T, Vitek MP, McKenna SE (2007) The novel apolipoprotein E-based peptide COG1410 improves sensorimotor performance and reduces injury magnitude following cortical contusion injury. J Neurotrauma 24:1108-1118.

Hodgetts S, Simmons P, Plant GW (2013a) Human mesenchymal precursor cells (Stro-1+) from spinal cord injury patients improve functional recovery and tissue sparing in an acute spinal cord injury rat model. Cell Transplantation 22:393-412.

Hodgetts SI, Simmons PJ, Plant GW (2013b) A comparison of the behavioral and anatomical outcomes in sub-acute and chronic spinal cord injury models following treatment with human mesenchymal precursor cell transplantation and recombinant decorin. Exp Neurol 248:343-359.

Hodgetts SI, Yoon JH, Fogliani A, Akinpelu E, Baron-Heeris D, Houwers IGJ, Wheeler L, Majda B, Santhakumar S, Lovett SJ, Duce E, Pollet M, Wiseman T, Fehily B, Harvey AR (2018) Cortical AAV-CNTF gene therapy combined with intraspinal mesenchymal precursor cell transplantation promotes functional and morphological outcomes after spinal cord injury in adult rats. Neural Plast 2018:9828725.
Hwang SR, Kim K (2014) Nano-enabled delivery systems across the blood-brain barrier. Arch Pharm Res 37:24-30.
Jiang Y, Brody DL (2012) Administration of COG1410 reduces axonal amyloid precursor protein immunoreactivity and microglial activation after controlled cortical impact in mice. J Neurotrauma 29:2332-2341.
Katoh H, Yokota K, Fehlings MG (2019) Regeneration of spinal cord connectivity through stem cell transplantation and biomaterial scaffolds. Front Cell Neurosci 13:248.
Kaufman NA, Beare JE, Tan AA, Vitek MP, McKenna SE, Hoane MR (2010) COG1410, an apolipoprotein E-based peptide, improves cognitive performance and reduces cortical loss following moderate fluid percussion injury in the rat. Behav Brain Res 214:395-401.
Kigerl KA, McGaughy VM, Popovich PG (2006) Comparative analysis of lesion development and intraspinal inflammation in four strains of mice following spinal contusion injury. J Comp Neurol 494:578-594.
Kumamaru H, Saiwai H, Ohkawa Y, Yamada H, Iwamoto Y, Okada S (2012) Age-related differences in cellular and molecular profiles of inflammatory responses after spinal cord injury. J Cell Physiol 227:1335-1346.
Kwon BK, Okon E, Hillyer J, Mann C, Baptiste D, Weaver LC, Fehlings MG, Tetzlaff W (2011) A systematic review of non-invasive pharmacologic neuroprotective treatments for acute spinal cord injury. J Neurotrauma 28:1545-1588.
Laskowitz DT, McKenna SE, Song P, Wang H, Durham L, Yeung N, Christensen D, Vitek MP (2007) COG1410, a novel apolipoprotein E-based peptide, improves functional recovery in a murine model of traumatic brain injury. J Neurotrauma 24:1093-1107.
MacDougall G, Anderton RS, Edwards AB, Knuckey NW, Meloni BP (2017) The Neuroprotective Peptide Poly-Arginine-12 (R12) Reduces cell surface levels of NMDA NR2B receptor subunit in cortical neurons; investigation into the involvement of endocytic mechanisms. J Mol Neurosci 61:235-246.
Maikos JT, Shreiber DI (2007) Immediate damage to the blood-spinal cord barrier due to mechanical trauma. J Neurotrauma 24:492-507.
McGowan JW, Bidwell GL, 3rd, Vig PJ (2015) Challenges and new strategies for therapeutic peptide delivery to the CNS. Ther Deliv 6:841-853.
Meloni BP, Craig AJ, Milech N, Hopkins RM, Watt PM, Knuckey NW (2014) The neuroprotective efficacy of cell-penetrating peptides TAT, penetratin, Arg-9, and Pep-1 in glutamic acid, kainic acid, and in vitro ischemia injury models using primary cortical neuronal cultures. Cell Mol Neurobiol 34:173-181.
Meloni BP, Milani D, Edwards AB, Anderton RS, O'Hare Doig RL, Fitzgerald M, Palmer TN, Knuckey NW (2015a) Neuroprotective peptides fused to arginine-rich cell penetrating peptides: Neuroprotective mechanism likely mediated by peptide endocytic properties. Pharmacol Ther 153:36-54.
Meloni BP, Milani D, Cross JL, Clark VW, Edwards AB, Anderton RS, Blacker DJ, Knuckey NW (2017) Assessment of the neuroprotective effects of arginine-rich protamine peptides, poly-arginine peptides (R12-Cyclic, R22) and arginine-tryptophan-containing peptides following in vitro excitotoxicity and/or permanent middle cerebral artery occlusion in rats. Neuromolecular Med 19:271-285.
Meloni BP, Brookes LM, Clark VW, Cross JL, Edwards AB, Anderton RS, Hopkins RM, Hoffmann K, Knuckey NW (2015b) Poly-arginine and arginine-rich peptides are neuroprotective in stroke models. J Cereb Blood Flow Metab 35:993-1004.
Metz GA, Whishaw IQ (2002) Cortical and subcortical lesions impair skilled walking in the ladder rung walking test: a new task to evaluate fore- and hindlimb stepping, placing, and co-ordination. J Neurosci Methods 115:169-179.
Milani D, Clark VW, Cross JL, Anderton RS, Knuckey NW, Meloni BP (2016) Poly-arginine peptides reduce infarct volume in a permanent middle cerebral artery rat stroke model. BMC Neurosci 17:19.
Milani D, Cross JL, Anderton RS, Blacker DJ, Knuckey NW, Meloni BP (2017) Neuroprotective efficacy of poly-arginine R18 and NA-1 (TAT-NR2B9c) peptides following transient middle cerebral artery occlusion in the rat. Neurosci Res 114:9-15.
Naqvi S, Panghal A, Flora SJS (2020) Nanotechnology: A promising approach for delivery of neuroprotective drugs. Front Neurosci 14:494.
Noble LJ, Wrathall JR (1989a) Correlative analyses of lesion development and functional status after graded spinal cord contusive injuries in the rat. Exp Neurol 103:34-40.
Noble LJ, Wrathall JR (1989b) Distribution and time course of protein extravasation in the rat spinal cord after contusive injury. Brain Res 482:57-66.
Plummer S, Van den Heuvel C, Thornton E, Corrigan F, Cappai R (2016) The neuroprotective properties of the amyloid precursor protein following traumatic brain injury. Aging Dis 7:163-179.
Plummer SL, Corrigan F, Thornton E, Woenig JA, Vink R, Cappai R, Van Den Heuvel C (2018) The amyloid precursor protein derivative, APP96-110, is efficacious following intravenous administration after traumatic brain injury. PLoS One 13:e0190449.
Popovich PG, Wei P, Stokes BT (1997) Cellular inflammatory response after spinal cord injury in Sprague-Dawley and Lewis rats. J Comp Neurol 377:443-464.
Popovich PG, Horner PJ, Mullin BB, Stokes BT (1996) A quantitative spatial analysis of the blood-spinal cord barrier. I. Permeability changes after experimental spinal contusion injury. Exp Neurol 142:258-275.
Qin X, You H, Cao F, Wu Y, Peng J, Pang J, Xu H, Chen Y, Chen L, Vitek MP, Li F, Sun X, Jiang Y (2017) Apolipoprotein E mimetic peptide increases cerebral glucose uptake by reducing blood-brain barrier disruption after controlled cortical impact in mice: An (18)F-fluorodeoxyglucose PET/CT study. J Neurotrauma 34:943-951.
Schnell L, Fearn S, Klassen H, Schwab ME, Perry VH (1999) Acute inflammatory responses to mechanical lesions in the CNS: differences between brain and spinal cord. Eur J Neurosci 11:3648-3658.
Shariati SA, Lau P, Hassan BA, Muller U, Dotti CG, De Strooper B, Gartner A (2013) APLP2 regulates neuronal stem cell differentiation during cortical development. J Cell Sci 126:1268-1277.
Siddiqui AM, Khazaei M, Fehlings MG (2015) Translating mechanisms of neuroprotection, regeneration, and repair to treatment of spinal cord injury. Prog Brain Res 218:15-54.
Small DH, Nurcombe V, Reed G, Clarris H, Moir R, Beyreuther K, Masters CL (1994) A heparin-binding domain in the amyloid protein precursor of Alzheimer's disease is involved in the regulation of neurite outgrowth. J Neurosci 14:2117-2127.
Soblosky JS, Colgin LL, Chorney-Lane D, Davidson JF, Carey ME (1997) Ladder beam and camera video recording system for evaluating forelimb and hindlimb deficits after sensorimotor cortex injury in rats. J Neurosci Methods 78:75-83.
Sroga JM, Jones TB, Kigerl KA, McGaughy VM, Popovich PG (2003) Rats and mice exhibit distinct inflammatory reactions after spinal cord injury. J Comp Neurol 462:223-240.
Sutherland TC, Mathews KJ, Mao Y, Nguyen T, Gorrie CA (2016) Differences in the cellular response to acute spinal cord injury between developing and mature rats highlights the potential significance of the inflammatory response. Front Cell Neurosci 10:310.
Swarup VP, Mencio CP, Hlady V, Kuberan B (2013) Sugar glues for broken neurons. Biomol Concepts 4:233-257.
Tetzlaff W, Okon EB, Karimi-Abdolrezaee S, Hill CE, Sparling JS, Plemel JR, Plunet WT, Tsai EC, Baptiste D, Smithson LJ, Kawaja MD, Fehlings MG, Kwon BK (2011) A systematic review of cellular transplantation therapies for spinal cord injury. J Neurotrauma 28:1611-1682.
Tukhovskaya EA, Yukin AY, Khokhlova ON, Murashev AN, Vitek MP (2009) COG1410, a novel apolipoprotein-E mimetic, improves functional and morphological recovery in a rat model of focal brain ischemia. J Neurosci Res 87:677-682.
Van den Heuvel C, Blumbergs PC, Finnie JW, Manavis J, Jones NR, Reilly PL, Pereira RA (1999) Upregulation of amyloid precursor protein messenger RNA in response to traumatic brain injury: an ovine head impact model. Exp Neurol 159:441-450.
Wang P, Yang G, Mosier DR, Chang P, Zaidi T, Gong YD, Zhao NM, Dominguez B, Lee KF, Gan WB, Zheng H (2005) Defective neuromuscular synapses in mice lacking amyloid precursor protein (APP) and APP-Like protein 2. J Neurosci 25:1219-1225.
Webb AA, Muir GD (2003) Unilateral dorsal column and rubrospinal tract injuries affect overground locomotion in the unrestrained rat. Eur J Neurosci 18:412-422.
Weyer SW, Klevanski M, Delekate A, Voikar V, Aydin D, Hick M, Filippov M, Drost N, Schaller KL, Saar M, Vogt MA, Gass P, Samanta A, Jaschke A, Korte M, Wolfer DP, Caldwell JH, Muller UC (2011) APP and APLP2 are essential at PNS and CNS synapses for transmission, spatial learning and LTP. EMBO J 30:2266-2280.
Yang L, Jones NR, Blumbergs PC, Van Den Heuvel C, Moore EJ, Manavis J, Sarvestani GT, Ghabriel MN (2005) Severity-dependent expression of pro-inflammatory cytokines in traumatic spinal cord injury in the rat. J Clin Neurosci 12:276-284.
Yokota K, Kobayakawa K, Kubota K, Miyawaki A, Okano H, Ohkawa Y, Iwamoto Y, Okada S (2015) Engrafted neural stem/progenitor cells promote functional recovery through synapse reorganization with spared host neurons after spinal cord injury. Stem Cell Reports 5:264-277.
Zhang B, Gensel JC (2014) Is neuroinflammation in the injured spinal cord different than in the brain? Examining intrinsic differences between the brain and spinal cord. Exp Neurol 258:112-120.
Zheng Y, Zhang YP, Shields LB, Zhang Y, Siu MW, Burke DA, Zhu J, Hu X, Dimar JR, Shields CB (2011) Effect of heparin following cervical spinal cord injuries in rats. Neurosurgery 69:930-941.

*C-Editors: Zhao M, Li CH; T-Editor: Jia Y*